5236

Microstructure characterisation of fixed prostate tissue using ultra high-resolution diffusion-weighted MRI

Maira Tariq[1], Andrada Ianus[1,2], Nyoman Kurniawan[3], Gary Cowin[4], Daniel C Alexander [1], Roger M Bourne[5], and Eleftheria Panagiotaki[1]

[1]Centre for Medical Image Computing, Department of Computer Science, University College London, London, United Kingdom, [2]Champalimaud Neuroscience Programme, Champalimaud Centre for the Unknown, Lisbon, Portugal, [3]Center for Advanced Imaging, University of Queensland, Brisbane, Australia, [4]National Imaging Facility, Queensland Node, Center for Advanced Imaging, University of Queensland, Brisbane, Australia, [5]Discipline of Medical Radiation Sciences, Faculty of Health Sciences, University of Sydney, Sydney, Australia

Synopsis

This work explores ultra-high field microimaging of prostate tissue using diffusion compartment modelling. The acquired ultra-high-resolution data provides a unique opportunity to investigate the accuracy of the diffusion estimates as well as the contribution of various tissue components to the diffusion signal. We compare several multi-compartment models to explore the best microstructure model for prostate tissue. We find plausible results for the data and models used, which will be compared to corresponding histology. Future work will use more samples and extend the models compared to get a comprehensive analysis of the data.

INTRODUCTION

In clinical prostate imaging the most common model for diffusion-weighted MRI (DW-MRI) is the mono-exponential model, which gives an apparent diffusion coefficient (ADC). But ADC is limited, as it cannot discriminate the specific histological features of the tissue. More sophisticated models that account for multiple microstructure components provide better characterisation of prostate tissue. For instance, VERDICT (Vascular, Extracellular, and Restricted Diffusion for Cytometry in Tumours) MRI provides a framework combining rich DW-MRI acquisition with a multi-compartment model to give non-invasive estimates of cancer tissue microstructure. Recent work demonstrates the potential of VERDICT for prostate imaging, to differentiate cancer and benign tissue, as well as cancer grading[1,2].

Several studies compare such models in terms of quality of fit and variance of the fitted parameters[3,4]. Some consensus exists in the models that can best describe the signal from prostate tissue, however, typical resolution of such studies is not sufficient to relate various components of these models to specific microstructure. Diffusion microimaging[5] provides spatial resolution approaching the cellular scale, which can be used to investigate the diffusion properties of different tissue types as shown in[6,7]. In this work we use diffusion microimaging with a richer protocol, to explore various multi-compartment models and determine ones that best characterise prostate tissue.

METHODS:

Three 3mm diameter x 4mm long samples (Figure.1a) of human prostate tissue (2 normal, 1 cancerous) were extracted from fixed radical prostatectomy specimens, with informed consent and ethics approval, as done in[6].

MR microimaging

MRI data were acquired on a Bruker 16.4T AVANCE II scanner, with a rich imaging protocol (Figure 1b). The DW-MRIs were acquired with a PGSE sequence with $(80\mu m)^3$ isotropic resolution, with multiple b-values and diffusion times to support estimation of various multi-compartment models. Two non diffusion-weighted images and three gradient orientations were sampled for each combination of acquisition parameters. A higher resolution $(20\mu m)^3$ T1/T2*-weighted image was also acquired for anatomical reference.

Data analysis

Fifteen models were fitted to the data, comprising 1, 2 or 3 compartments as listed in Figure 2a. For ex-vivo data there is no perfusion component in prostate tissue, but we tested 3-compartment models as the high-resolution data may enable separation of further non-perfusion components of the tissue. The models compared were combinations of sphere, stick, ball, and zeppelin compartments (terminology as in[8]), and included the conventionally used cancer models: ADC (Ball) and bi-exponential (BallBall). Model fitting was performed using the non-linear fitting procedure used in[1], with data normalised using the b=0 data for each echo time, to account for T2 dependence. The models were fitted without fixing any model parameters.

Regions-of-interest (ROIs) were drawn on the DW-MRIs, by manually selecting areas composed primarily of a single tissue type, as shown in Figure.2b. We specifically included glandular and stromal tissue for normal samples and cancer tissue, by finding visual correspondence to the higher-resolution T2*-MRIs where histological features are moderately well visible (histological confirmation with stained sections is not yet available). Model fitting was done for the signal averaged over these ROIs, for all the models. The models were then ranked based on the Bayesian Information Criterion (BIC)[9]. Voxel-wise model fitting was also performed to extract maps of microstructure parameters.

RESULTS:

ROI analysis

Figure 3 shows that multi-compartment models best explain the acquired data and 2-compartment models with restriction perform the best overall. The best-ranked models show that regions of cancer and glandular tissue are best described by a model with isotropic restriction, while stromal tissue requires anisotropy. The corresponding parameter estimates for the best ranking models (Figure 3b) show a higher restriction compartment in the cancer ROIs compared to normal ROIs, as expected.

Voxel-wise analysis

Figure 4 shows the variation of the model ranking for the top performing models in each sample. The trends are overall similar to the ROI analysis. Additionally, we find non-restriction model is sufficient in areas with lumen space. The parameter maps corresponding to BallSphere, the best performing model, is shown in Figure 5, which show plausible trends.

DISCUSSION AND CONCLUSION:

This work explores separation of the various tissue compartments in prostate samples with DW-MRIs acquired on an ultra-high field scanner. We see that with diffusion microimaging, we can explore the specific components of the microstructure using multi-compartment models. However, none of the models used here fully capture the complexity of the data (Figure 3a). Incorporating more orientations in the DW-MRI acquisitions will improve the model fitting and provide better anisotropy characterisation. Future work will also investigate more complex models, including incorporation of T2 relaxation in modelling.

A bigger set of tissue samples are required for a comprehensive analysis to determine the best model that fully characterises the microstructure of normal and cancerous prostate tissue.

Acknowledgements

This work is funded by a grant PG14-018-TR2 from Prostate Cancer UK. EPSRC grant EP/N021967/1 supports EP's work on this topic, and EP/M020533/1 and EP/N018702/1 support DCA.

References

1. Panagiotaki, E. et al. Microstructural Characterization of Normal and Malignant Human Prostate Tissue With Vascular, Extracellular, and Restricted Diffusion for Cytometry in Tumours Magnetic Resonance Imaging. Invest. Radiol. 50, 218–227 (2015).

2. Johnston, E. et al. Short term repeatability of microstructural (VERDICT) MRI vs. ADC in prostate cancer. in ISMRM (2016).

3. Liang, S. et al. Information-based ranking of 10 compartment models of diffusion-weighted signal attenuation in fixed prostate tissue. NMR Biomed. 29, 660–671 (2016).

4. Bailey, C. et al. (ISMRM 2017) Validation of VERDICT MRI using fresh and fixed prostate specimens with aligned histological slices. in (2017).

5. Bourne, R., Kurniawan, N., Cowin, G., Sved, P. & Watson, G. 16 T diffusion microimaging of fixed prostate tissue: preliminary findings. Magn. Reson. Med. 66, 244–247 (2011).

6. Bourne, R. M. et al. Microscopic diffusivity compartmentation in formalin-fixed prostate tissue. Magn. Reson. Med. 68, 614–620 (2012).

7. Bourne, R. M. et al. Biexponential diffusion decay in formalin-fixed prostate tissue: Preliminary findings. Magn. Reson. Med. 68, 954–959 (2012).

8. Panagiotaki, E. et al. Compartment models of the diffusion MR signal in brain white matter: A taxonomy and comparison. NeuroImage 59, 2241–2254 (2012).

9. Schwarz, G. Estimating the Dimension of a Model. Ann. Stat. 6, 461–464 (1978).

10. Panagiotaki, E. et al. Noninvasive Quantification of Solid Tumor Microstructure Using VERDICT MRI. Cancer Res. 74, 1902–1912 (2014).

Figures

a)

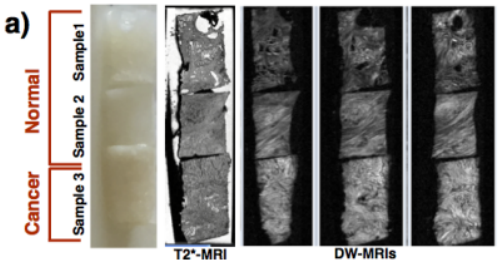

b)

Δ/δ (ms)	TE (ms)	b-value (s/mm^2)					
		200	500	1000	1600	2200	3000
20/5	31	78	132	179	223	263	302
40/5	51	54	91	124	154	182	209
80/5	91	38	64	87	108	127	146
10/2	22	274	462	627	780	923	1059
20/10	36	41	69	94	117	138	159
40/10	56	28	47	63	79	93	107

|G| (mT/m) values are shown for each gradient seperation, Δ and duration, δ.

Figure 1: a) the prostate samples and some example MRI acquisitions. b) table of the protocol used for the DW-MRI acquisition, which shows the gradient strengths, |G| (mT/m), which are varied to obtain each of the b-values, for each combination of gradient seperation and duration.

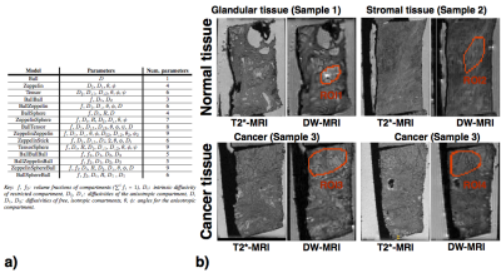

Figure 2: a) List of the compartment models included in the model comparison. The compartments are named using terminology in[10]. b) ROIs used in analysis, which are manually segmented to correspond to a single tissue or compartment type, using the corresponding structural image. The glandular tissue consists of a gland (epithelium + lumen space), the stromal tissue is likely fibrous. The cancer ROIs likely include epithelium, stroma, as well as lumen.

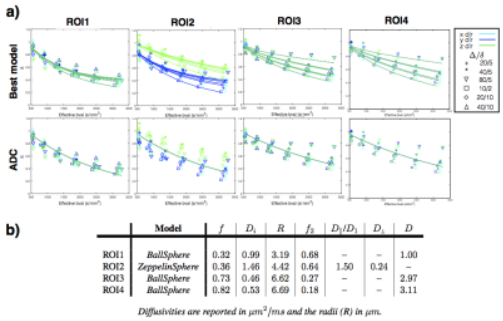

	Model	f	D_i	R	f_2	D_i/D_1	D_1	D
ROI1	*BallSphere*	0.32	0.99	3.19	0.68	–	–	1.00
ROI2	*ZeppelinSphere*	0.36	1.46	4.42	0.64	1.50	0.24	–
ROI3	*BallSphere*	0.73	0.46	6.62	0.27	–	–	2.97
ROI4	*BallSphere*	0.82	0.53	6.69	0.18	–	–	3.11

Diffusivities are reported in $\mu m^2/ms$ and the radii (R) in μm.

Figure 3: a) Plots of the synthesised signal from the estimated parameters (lines), for the best models according to BIC, and the ADC, for each ROI (Figure.2) The colours indicate the different gradient orientations and the symbols the particular combination of gradient separation and duration, as specified. b) The estimated parameters for the best-ranked model (according to the BIC) for each of the ROIs.

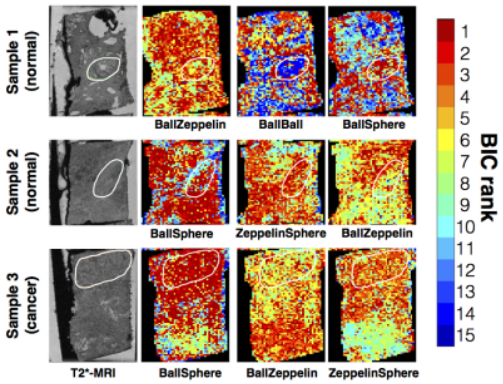

Figure 4: BIC Model rankings for the top three models for each of the tissue samples. The contours on the images show glandular, stromal and cancer tissue in this slice, to highlight similarity to the findings from the ROI analysis.

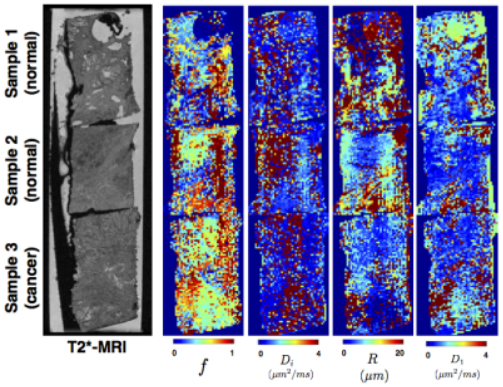

Figure 5: Estimated parameters maps for voxel-wise fit for BallSphere in a slice of DW-MRI data. The corresponding T2*-MRI is shown on the left for reference. These parameter maps include the volume fraction, f, of the restriction compartment and the associated intrinsic diffusivity (D_i) and the radius estimates (R), as well as the diffusivity of the non-restriction compartment (D_1).